

## Calculation of ionization within the close-coupling formalism

Igor Bray\* and Dmitry V. Fursa

*Electronic Structure of Materials Centre, The Flinders University of South Australia, G.P.O. Box 2100, Adelaide 5001, Australia*

(Received 7 May 1996)

We present a method for calculation of differential ionization cross sections from theories that use the close-coupling expansion for the total wave function. It is shown how, from a single such calculation, elastic, excitation, and ionization cross sections may be extracted using solely the  $T$ -matrix elements arising from solution of the coupled equations. To demonstrate the applicability of this formalism, the convergent close-coupling theory is systematically applied at incident energies of 150–600 eV to the calculation of  $e$ -He ionization. Comparison with available measurements is generally very good. [S1050-2947(96)11209-9]

PACS number(s): 34.80.Bm, 34.80.Dp

### I. INTRODUCTION

Our primary motivation in developing electron-atom (or ion) scattering theory is to provide data useful for practical and scientific applications. For this purpose, we desire a general theory that yields accurate results irrespective of the projectile energy or the scattering process of interest. By analogy to the concept of a complete, scattering experiment, one that measures all aspects of a particular scattering process, [1,2] such a theory could be referred to as a “complete” scattering theory. It is our goal to extend the convergent close-coupling (CCC) method, introduced by Bray and Stelbovics [3], to fulfill these criteria, and to extend its applicability to a large range of targets.

These goals are easy to state but difficult to achieve. Electron-atom collisions consist of a big variety of scattering processes. If the energy of the projectile is above the ionization threshold, then elastic, excitation, and ionization processes occur. These interfere and compete with each other and hence as many as possible should be taken into account in the scattering theory. The close-coupling (CC) formalism is designed with this aim in mind, and is particularly suited to the treatment of discrete excitations. However, historically the target continuum has been completely left out of the CC calculations, yielding identically zero for ionization cross sections, which has been the major factor in limiting the generality of the CC approach. In relatively recent times, many CC calculations have been extended to incorporate the treatment of the target continuum via the use of pseudostates; see, for example [3–7], and references therein. These states are obtained by diagonalizing the target Hamiltonian in some square-integrable basis, with the positive-energy states providing a discretized representation of the target continuum.

The introduction of pseudostates to the CC formalism considerably improved agreement between theory and experiment for the discrete transitions, and allowed for the application of such calculations at all energies of interest. Problems with pseudo-resonances that typically plagued the early applications were shown to be primarily due to an insufficient basis size used in the calculation [8]. Generally, we argue that for the purpose of calculating discrete excitations,

a treatment of the target continuum provided by pseudostates is sufficiently accurate for practical applications; see, for example [9,10], in the cases of  $e$ -Na and  $e$ -He scattering, respectively.

In order to demonstrate that a scattering theory is complete, the treatment of the target continuum needs to be directly applied to the calculation of ionization processes. The strength of the CC approach with pseudostates to ionization is that it allows for the treatment of the discrete transitions when calculating ionization in the same way that the continuum is taken into account when calculating discrete transitions. Furthermore, unitarity of the CC formalism allows for an immediate test of the calculation by applying it to the least detailed ionization process, namely, the total ionization cross section. Unitarity ensures that this cross section converges rapidly with increasing number of states. In particular, the target-space expansions do not require large orbital angular momenta [11].

The first indication that one should be able to obtain accurate ionization information from the CCC theory was provided by application to the calculation of electron-impact total ionization cross sections and the associated spin asymmetries of atomic hydrogen [12]. This indicated that the theory correctly predicted the spin-dependent distribution of electron flux between the discrete and continuum channels. Even though the total ionization cross section is the least detailed parameter used to describe ionization, we shall see that obtaining these by the CCC method has surprising implications for our formal ionization theory.

The CCC theory has already been applied to the more detailed triple-differential ionization cross section [13–15]. The idea is much the same as that applied initially by Curran and Walters [16] and by Curran, Whelan, and Walters [17], namely, to use a CC representation of the total wave function. There are, however, some notable differences in our approach that lead to substantial simplification. In the CCC theory, the ionization amplitudes are generated directly from the  $T$ -matrix elements arising from the solution of the CC equations.

The aim of this paper is to explain how we obtain detailed ionization information from the CCC theory. This includes total, single-, double-, and triple-differential ionization cross sections. We have already demonstrated that a single calculation yields these cross sections accurately in the case of

\*Electronic address: I.Bray@flinders.edu.au

$e$ -He scattering at 100 eV [18]. Here we concentrate on energies above 100 eV, where there are an abundance of experimental data for the various differential ionization cross sections.

## II. THEORY

The details of the CCC theory for the case of hydrogenic targets have been given by Bray and Stelbovics [19], and for the case of helium by Fursa and Bray [10]. These discuss techniques for defining and solving the coupled equations in the CCC formalism. Applying the method to ionization requires revisiting the foundations of the CCC theory, and we shall focus our attention in this area.

In this paper we shall only concern ourselves with the case where ionization involves ejection of only one target electron. Core excitation or ionization is explicitly excluded from our formalism, as is two-electron ejection by electron impact. Implicitly, we have in mind ‘‘one-electron’’ targets such as H, Li, Na, and the He atom treated by the frozen-core approximation. Unless stated otherwise, atomic units will be used throughout.

### A. Formal CCC theory

In the CCC method, we do not directly solve the Schrödinger equation

$$(H - E)|\Psi_i^{(+)}\rangle = 0, \quad (1)$$

where  $E$ ,  $H$ , and  $\Psi_i$  are the total energy, Hamiltonian, and wave function (with incoming plane-wave and outgoing spherical-wave boundary conditions), respectively. Instead, we solve for the  $T$  matrix

$$T_{\text{fi}} = \langle \Phi_f | H - E | \Psi_i^{(+)} \rangle, \quad (2)$$

where  $\Phi_f$  is the asymptotic wave function and  $H = K + V$  is defined as acting on the left-hand side. At this stage we do not specify the asymptotic Hamiltonian  $K$ , its eigenstates  $\Phi_f$ , or the interaction potential  $V$ . We shall find that they will be determined by the method of solution.

Since it is numerically difficult to work with functions obeying explicit symmetry conditions, we write

$$|\Psi_i^{(+)}\rangle = (1 - P_{\text{rs}})|\psi_i^{(+)}\rangle, \quad (3)$$

where the operator  $1 - P_{\text{rs}}$  ensures antisymmetry upon interchange of spatial coordinates and spin, in the total wave function for any unsymmetrized function  $\psi_i^{(+)}$ . Note that this expansion is at the cost of a nonunique determination of  $\psi_i^{(+)}$ . In the CCC method, this expansion introduces numerical instabilities that need to be addressed [20]. Equation (2) now becomes

$$T_{\text{fi}} = \langle \Phi_f | H - E + (E - H)P_{\text{rs}} | \psi_i^{(+)} \rangle. \quad (4)$$

To solve (4) we first obtain a set of square-integrable target states by diagonalizing the target Hamiltonian  $H_T$  in an orthogonal Laguerre basis of size  $N$ . The  $N$  resulting states satisfy

$$\langle \phi_m^N | H_T | \phi_n^N \rangle = \epsilon_n^N \delta_{mn}. \quad (5)$$

As the basis size  $N$  is increased, the negative-energy (above a frozen core) states converge pointwise to the discrete target eigenstates, whereas the positive-energy states provide an increasingly dense discretization of the target continuum. An expansion involving a summation over the positive-energy states is equivalent to an integration over the true target continuum states [21]. We model hydrogenic targets as one active electron above a frozen Hartree-Fock core [9]. For helium, we include only the configurations where one of the target electrons is represented by the  $1s$  orbital of  $\text{He}^+$  [10]. The target-state energies may then be defined relative to the core and then excitation of states with negative energies corresponds to discrete transitions, while excitation of states with positive energies ( $\epsilon_q = q^2/2$ ) corresponds to ionization of the target.

Having defined our target states, we use them to form the multichannel expansion of the unsymmetrized wave function  $\psi_i^{(+)}$ . We define the projection operator  $I^N$  by

$$I^N = \sum_{n=1}^N |\phi_n^N\rangle \langle \phi_n^N|, \quad (6)$$

with the use of an orthogonal Laguerre basis ensuring that  $\lim_{N \rightarrow \infty} I^N = I$ , the true identity operator acting in the space of the target electron(s). We approximate the  $T$  matrix (4) by using a finite basis expansion of the target space,

$$T_{\text{fi}} \approx T_{\text{fi}}^N = \langle \Phi_f | I^N | H - E + (E - H)P_{\text{rs}} | I^N \psi_i^{(+)} \rangle. \quad (7)$$

Note that we used  $I^N$  on both sides to ensure that the target space is confined to the Hilbert space spanned by our target states  $\phi_n^N$ . This way we do not have any problems with non-existent integrals of the kind discussed by Curran and Walters [16]. Furthermore, it is this expansion that determines the asymptotic Hamiltonian  $K$ . By construction we have ensured that the target-space functions always vanish for sufficiently large radial coordinates. This means that asymptotically the projectile must be treated as a plane wave, with the motion of the target electrons being governed solely by the target Hamiltonian. Hence, we write the asymptotic Hamiltonian as

$$K = K_0 + H_T, \quad (8)$$

where  $K_0$  is the free one-electron Hamiltonian (we use the subscript 0 to denote projectile space). As a consequence, the asymptotic states  $\Phi_f$  satisfy

$$(H_T + K_0 - E)|\Phi_f\rangle = 0, \quad (9)$$

and we may write  $\langle \Phi_f | = \langle \mathbf{k}_f \phi_f |$ , where  $\phi_f$  is an eigenstate (discrete or continuous) of  $H_T$  with energy  $\epsilon_f$ , and  $\mathbf{k}_f$  is a plane wave with energy  $k_f^2/2$  such that  $E = \epsilon_f + k_f^2/2$ . In practice we add a short-ranged projectile-space distorting potential  $U_0$  to (9) and work with distorted waves  $\mathbf{k}_f^{(\pm)}$ . However, this is used purely for reducing computational requirements, and our results are independent of the choice of this potential. For clarity of presentation we choose the plane-wave notation here. See Ref. [9] for more detail regarding the usage of  $U_0$  in CCC calculations.

If we take  $\phi_f$  such that  $\epsilon_f = \epsilon_n^N$  for some  $n = 1, \dots, N$ , then, using (5), the  $T$  matrix (7) becomes

$$\begin{aligned}
T_{fi}^N &= \sum_{n=1}^N \langle \phi_f | \phi_n^N \rangle \langle \mathbf{k}_f \phi_n^N | \epsilon_n^N + K_0 + V - E + (E - H) P_{rs} | I^N \psi_i^{(+)} \rangle \\
&\approx \sum_{n: \epsilon_n^N = \epsilon_f} \langle \phi_f | \phi_n^N \rangle \langle \mathbf{k}_f \phi_n^N | V + (E - H) P_{rs} | I^N \psi_i^{(+)} \rangle \equiv \sum_{n: \epsilon_n^N = \epsilon_f} \langle \phi_f | \phi_n^N \rangle \langle \mathbf{k}_n \phi_n^N | T | \phi_i^N \mathbf{k}_i \rangle.
\end{aligned} \quad (10)$$

Note that by energy conservation we may write in (10)  $\mathbf{k}_f = \mathbf{k}_n$ . The approximation comes from the fact that for a sufficiently large  $N$  the overlaps  $\langle \phi_f | \phi_n^N \rangle$  are essentially zero if  $\epsilon_n^N \neq \epsilon_f$ ; otherwise this overlap is unity in the case of discrete excitation, and in the case of ionization it monotonically increases with the size of the basis. The summation, in the case of ionization, is just a sum over the orbital angular momenta of states with the same energy as the continuum wave  $\phi_f$ .

For all of the square-integrable target states  $\phi_n^N$  ( $n=1, \dots, N$ ), the CCC calculations [3,9,10] yield  $T$ -matrix elements occurring in (10), independent of the choice of the distorting potential  $U_0$ , by solving the coupled Lippmann-Schwinger equations

$$\langle \mathbf{k}_n \phi_n^N | T | \phi_i^N \mathbf{k}_i \rangle = \langle \mathbf{k}_n \phi_n^N | V + (E - H) P_{rs} | \phi_i^N \mathbf{k}_i \rangle + \sum_{m=1}^N \int d\mathbf{k} \frac{\langle \mathbf{k}_n \phi_n^N | V + (E - H) P_{rs} | \phi_m^N \mathbf{k} \rangle \langle \mathbf{k} \phi_m^N | T | \phi_i^N \mathbf{k}_i \rangle}{E + i0 - \epsilon_m^N - k^2/2}. \quad (11)$$

The basis size  $N$  is progressively increased until convergence in (10) is obtained to a desired accuracy. Obtaining convergence in the ionization case is particularly encouraging since the overlap  $\langle \phi_f | \phi_n^N \rangle$  ( $\epsilon_n^N = \epsilon_f$ ) tends to infinity with increasing  $N$ . This overlap may be interpreted as restoring the continuum normalization and boundary conditions to the square-integrable positive-energy (above-core) state  $\phi_n^N$ .

Now let us consider in some detail the consequences for the calculation of ionization. The multichannel expansion may be written explicitly as

$$|I^N \psi_i^{(+)}\rangle = \sum_{n=1}^N |\phi_n^N f_{ni}^{(+)}\rangle, \quad (12)$$

where  $|f_{ni}^{(+)}\rangle = \langle \phi_n^N | \psi_i^{(+)} \rangle$  are one-electron functions. The square-integrability of our target states ensures that there is only one electron at true infinity. This way we avoid the complicated considerations involving divergent phase factors [22]. Clearly, there is no room for the three-body boundary conditions [23]. In other words, imposition of the multichannel expansion induces a target-space ‘‘box’’ on the scattering system from which only the projectile-space electron is allowed to escape. The overlap in (10) is a way of propagating outside the box the single positive-energy target-space electron in the potential of the residual ion. The projectile-space electron propagates asymptotically as a plane wave with the nucleus being totally shielded by the target-space electron(s). Note that this interpretation assumes nothing about the relative energies of the projectile- and target-space electrons. Furthermore, the projectile- and target-space electrons are distinguishable (we may refer to the projectile-space electron as the primary electron and to the continuum target-space electron as the ejected electron). Therefore, channels  $m$  and  $n$ , where the final energies are such that  $\epsilon_m^N = k_m^2/2$ , and so  $\epsilon_n^N = k_n^2/2$ , belong to theoretically distinguishable processes. As these are not distinguished in measurements, we sum the cross section for each of these transitions. However, the amplitudes for these individual transitions are made from a co-

herent sum of the direct  $V$  and the exchange  $(E - H)P_{rs}$  terms. We shall elaborate on this further when defining the cross sections for comparison with experiment.

A simple example of the necessity to interpret the projectile- and target-space electrons as being distinguishable is provided by attempting to define the total ionization cross section. The CCC theory is unitary, and so the total cross section  $\sigma_i$  may be obtained from the forward elastic scattering amplitude as well as by simply summing the cross section corresponding to excitation of all states included in the multichannel expansion. Since we know that the negative-energy states converge, with increasing  $N$ , to the true discrete eigenstates, the total nonbreakup cross section  $\sigma_{nb}$  is defined as the sum of the cross sections corresponding to excitation of only the negative-energy states. The total ionization cross section  $\sigma_i = \sigma_i - \sigma_{nb}$  is also given by taking the sum of cross sections corresponding to excitation of only the positive-energy (above-core) states. This sum correctly predicts  $\sigma_i$  [12], and contains terms with  $\epsilon_n^N < E/2$  and  $\epsilon_n^N > E/2$ , without any double-counting problems (see [24] for more details). In other words, the CCC theory obtains the total ionization cross section as an integral from 0 to  $E$ , whereas experimentally this is obtained by integrating the measured single-differential ionization cross section (which is symmetric about  $E/2$ ) from 0 to  $E/2$ .

An important practical consequence of our formulation for the calculation of ionization is that we may use the  $T$ -matrix elements arising from the solution of the coupled equations without modification of the CCC formalism used for discrete excitation. All we require is the calculation of the true target continuum waves at the same energies as the square-integrable target states. In order to make comparison with experiment, however, we may need to interpolate the obtained  $T$ -matrix elements to the energies measured in the experiment. Though this does introduce some extra numerical uncertainty, such interpolation allows a single CCC calculation to yield single-, double-, and triple-differential ionization cross sections for any energy-sharing combination of the two outgoing electrons of the total energy  $E$ .

## B. Calculation of the ionization amplitudes

The  $T$ -matrix equation (11) is solved by expanding the  $T$  matrix in partial waves  $J$  of the total orbital angular mo-

mentum, total spin  $S$ , and parity  $\Pi$ . The resulting reduced  $T$ -matrix elements  $T_{ni}^{J,S,\Pi,N}$  are used to calculate the scattering amplitudes for each state (as required) included in the multichannel expansion

$$f_{n_s n_l n m_n, i s_l i m_i}^{SN}(\theta, \varphi) \equiv \langle \mathbf{k}_n \phi_n^N | T^{SN} | \phi_i^N \mathbf{k}_i \rangle$$

$$= \frac{1}{\sqrt{4\pi}} \frac{1}{\sqrt{2l_i+1}} \sqrt{\frac{k_i}{k_n}} \sum_{L_n, L_i, J, \Pi} \sqrt{2L_i+1} C_{L_n}^{m_i - m_n m_n m_i} C_{L_i}^{0 m_i m_i} T_{s_n n_l n s_l i l_i}^{J,S,\Pi,N} Y_{m_i - m_n}^{L_n}(\theta, \varphi), \quad (13)$$

where  $l_i, m_i$  and  $l_n, m_n$  are the orbital angular momenta and their projections of the initial and final atom states, respectively. The initial and final linear and orbital angular momenta of the projectile are denoted by  $k_i, L_i$  and  $k_n, L_n$ . The quantization axis is chosen along the incident projectile direction. We use the spin-coupled form for the total projectile-target electron wave function with  $s_n$  and  $s_i$  indicating the spins of the final and initial states of the target atom, respectively. In the following we will drop the initial-state indices for brevity of presentation whenever no ambiguity arises. In particular, we write (13) as  $f_{nslm}^{SN}(\theta, \varphi) \equiv f_{slm}^{SN}(\mathbf{k})$ , where  $s, l, m$  denotes the final state indices. Note that  $\mathbf{k} = \mathbf{k}_n = \mathbf{k}_f$ .

The scattering amplitudes may be calculated for negative-energy (above-core) states as well as for positive energy states. In the former case they are used to obtain all experimentally observable quantities characterizing discrete spectrum excitations (such as various cross sections and electron-impact coherence parameters). In the latter case,  $\epsilon_f = \epsilon_q > 0$ ,  $\phi_f \equiv \mathbf{q}_s^{(-)}$  ( $s$  is the spin of the target continuum wave with momentum  $\mathbf{q}$ ), they are used to make the  $e$ -2e ionization amplitude (10)

$$f_s^{SN}(\mathbf{k}, \mathbf{q}) = \sum_{n: \epsilon_n^N = \epsilon_f} \langle \mathbf{q}_s^{(-)} | \phi_n^N \rangle \langle \mathbf{k}_n \phi_n^N | T^{SN} | \phi_i^N \mathbf{k}_i \rangle$$

$$= \sum_{lm} (-i)^l \exp(i\sigma_l) Y_{lm}(\hat{\mathbf{q}}) f_{slm}^{SN}(\mathbf{k}, \mathbf{q}), \quad (14)$$

where the amplitudes  $f_{slm}^{SN}(\mathbf{k}, \mathbf{q})$  are given by

$$f_{slm}^{SN}(\mathbf{k}, \mathbf{q}) = \langle \phi_q^{slm} | \phi_n^{Nslm} \rangle f_{slm}^{SN}(\mathbf{k}), \quad (15)$$

and where  $\phi_n^{Nslm}$  is the state  $\phi_n^{Nslm}$  with energy  $\epsilon_n^N = \epsilon_q$ . Here we have used the partial-wave expansion of the continuum wave

$$\mathbf{q}_s^{(\pm)} = \sum_{lm} i^l \exp(\pm i\sigma_l) Y_{lm}^*(\hat{\mathbf{q}}) \phi_q^{slm}, \quad (16)$$

where  $\sigma_l$  is the Coulomb phase shift, and the continuum functions  $\phi_q^{slm}$  will be determined later. Note that only one target-space electron of  $\phi_q^{slm}$  is in the continuum. The rest, if any, are frozen in the inert target core.

## 1. Interpolation

As mentioned above, we require the energy of the continuum wave  $\epsilon_q$  in (15) to be the same as that of one of the pseudostates  $\epsilon_n^N$ . However, in practice it is the experiment that determines the value  $\epsilon_q$ , and so for each set of target quantum numbers  $l, s$  we need to generate our pseudostates to yield a state with energy  $\epsilon_n^N = \epsilon_q$ . In the case of quasi-one-electron targets ( $s = 1/2$ ), we may readily obtain the required energy for each  $l$  by slightly varying the exponential falloff of the Laguerre basis [13]. In the case of quasi-two-electron targets ( $s = 0, 1$ ) this is more difficult. Furthermore, in either case we may have a number of experiments for a given incident energy with different  $\epsilon_q$ , making it impossible to match these to the available  $\epsilon_n^N$  arising in a single CCC calculation. We therefore devise an interpolation scheme of the positive-energy  $T$ -matrix elements so as to be able to obtain the required scattering amplitudes (15) at any energy  $0 < \epsilon_q < E$ .

For each partial wave  $J$  and total spin  $S$ , upon solving the coupled equations we obtain complex matrix elements  $T_{s_n n_l n}^{J,S,\Pi,N}$  corresponding to excitation of positive-energy pseudostates with  $0 < \epsilon_n^N < E$ . We first put the matrix elements onto the continuum scale by multiplying them by the overlaps (15) with the continuum functions evaluated at  $\epsilon_q = \epsilon_n^N$ . We then interpolate the absolute, real, and imaginary parts separately onto the energies at which experimental data are available. The interpolation over the absolute values is used to renormalize the individual real and imaginary parts, which ensures that we obtain similar partial integration cross sections by either summing over partial cross sections for positive-energy states or integrating ( $de$  from 0 to  $E$ ) over the results interpolated onto the continuous scale. This allows for a check of the interpolation for each  $l, s$  target quantum numbers within each partial wave  $J$ .

Another way to obtain the amplitudes at the required energies is to first calculate the amplitudes for each of the open pseudostates, and then interpolate these instead of the  $T$ -matrix elements. This has the advantage that we may include the ‘‘Born subtraction’’ (see [25], for example) for each amplitude, thereby taking care of the high partial waves. It may also be a more accurate interpolation procedure at some scattering angles, though we do lose the above-mentioned direct check when interpolating the  $T$ -matrix elements. Most importantly, the two schemes serve as a check

of the interpolation choice on the results of a single CCC calculation.

With the aid of the interpolation schemes, ionization cross sections for any kinematic region of the two outgoing electrons may be generated after the completion of a single CCC calculation. Generally, the quality of the interpolation depends on the number of pseudostate energies surrounding the required energy. This becomes particularly important in the equal energy sharing region and for large total energies  $E$ . In these cases we find it important to have an energy level close to  $E/2$  for each  $l, s$  combination. By increasing the basis size we vary all of the energy levels, and so simultaneously check for stability of the results as a function of basis size and quality of interpolation.

## 2. Calculation of the continuum waves

In the case of the hydrogen target the continuum waves are pure Coulomb waves, which are calculated in a way similar to the projectile continuum partial-wave calculation (solving the one-dimensional differential equation). For hydrogenic targets we obtain the one-electron continuum target states by solving the frozen-core Hartree-Fock equations [26]. Finally, for the helium target we do the following.

Continuum helium target states with spin  $s$  in the frozen-core approximation are given by

$$\begin{aligned} \chi_s^{(\pm)}(x_1, x_2) = & \frac{1}{\sqrt{2}} \left( \frac{1}{r_1} u(r_1) \chi_s^{(\pm)}(\mathbf{q}, \mathbf{r}_2) \right. \\ & \left. + \frac{(-1)^s}{r_2} u(r_2) \chi_s^{(\pm)}(\mathbf{q}, \mathbf{r}_1) \right) X(s), \end{aligned} \quad (17)$$

where  $x$  denotes coordinate and spin space,  $X(s)$  is a two-electron spin function [see Eq. (10) in Ref. [10]], and  $u(r)$  is the He<sup>+</sup> 1s orbital. The function  $\chi_s^{(\pm)}(\mathbf{q}, \mathbf{r})$  is a one-electron continuum wave

$$\chi_s^{(\pm)}(\mathbf{q}, \mathbf{r}) = \sqrt{\frac{2}{\pi}} \frac{1}{qr} \sum_{l, m} i^l \exp(\pm i\sigma_l) u_{sl}(q, r) Y_{lm}^*(\hat{\mathbf{q}}) Y_{lm}(\hat{\mathbf{r}}), \quad (18)$$

where  $\sigma_l$  is the Coulomb phase shift.

Using (18), the partial-wave expansion for the two-electron continuum wave (17) can be written as

$$\chi_s^{(\pm)}(x_1, x_2) = \sum_{l, m} i^l \exp(\pm i\sigma_l) Y_{lm}^*(\hat{\mathbf{q}}) \phi_q^{slm}(\mathbf{r}_1, \mathbf{r}_2) X(s), \quad (19)$$

where

$$\begin{aligned} \phi_q^{slm}(\mathbf{r}_1, \mathbf{r}_2) = & \frac{1}{\sqrt{\pi}qr_1r_2} [u(r_1)u_{sl}(q, r_2)Y_{lm}(\hat{\mathbf{r}}_2) \\ & + (-1)^s u(r_2)u_{sl}(q, r_1)Y_{lm}(\hat{\mathbf{r}}_1)]. \end{aligned} \quad (20)$$

The radial function  $u_{sl}(q, r)$  is the solution of the frozen-core Hartree-Fock equation [27]

$$\begin{aligned} \frac{d^2}{dr^2} u_{sl} - \left[ \frac{l(l+1)}{r^2} - \frac{2Z}{r} + 2Y^0(u, u) - 2\epsilon_q \right] u_{sl} \\ = \left[ (-1)^s \frac{2}{2l+1} Y^l(u, u_{sl}) - 2\lambda \right] u, \end{aligned} \quad (21)$$

where  $Z=2$ ,  $\epsilon_q = q^2/2 = E - k_n^2/2 + 2$  is the energy of the one-electron continuum wave (the corresponding two-electron continuum wave has the energy  $e = q^2/2 - 2$ ), where  $-2$  a.u. is the energy of the He<sup>+</sup> ground state, and

$$Y^l(f, g) = \frac{1}{r^{l+1}} \int_0^r f(t)g(t)t^l dt + r^l \int_r^\infty \frac{f(t)g(t)}{t^{l+1}} dt. \quad (22)$$

The coefficient  $\lambda$  is equal to zero for all <sup>1,3</sup>L symmetries except for the <sup>1</sup>S symmetry, where it is given by

$$\lambda = \int_0^\infty u(t)Y^0(u, u_{sl})u_{sl}(q, t)dt. \quad (23)$$

Equation (21) is of the general form

$$\begin{aligned} \frac{d^2}{dr^2} y(r) - f(r)y(r) = g(r, y), \\ g(r, y) = \int_0^\infty K(r, r')y(r')dr'. \end{aligned} \quad (24)$$

This is a linear integrodifferential equation and is solved by iteration as in the case of solving the Hartree-Fock equations [28]. The zero approximation  $y^{(0)}$  is obtained by taking  $g=0$  in (24). The consequent approximations are given by

$$\frac{d^2}{dr^2} y^{(n+1)} - f(r)y^{(n+1)} = g(r, y^{(n)}). \quad (25)$$

At each iteration the linear inhomogeneous second-order differential equation (25) for  $y^{(n+1)}$  is solved by the Numerov method. The iteration process converges quickly and only a few iterations are usually required to achieve accuracy ( $|y^{(n+1)}(r) - y^{(n)}(r)| < 10^{-5}, \forall r$ ).

The radial one-electron continuum function  $u_{sl}(q, r)$  is matched to Coulomb functions at large  $r$ . The two-electron continuum waves (17) are normalized to the  $\delta$  function in momentum space

$$\langle \mathbf{q}^{(\pm)} | \mathbf{q}'^{(\pm)} \rangle = \delta^3(\mathbf{q} - \mathbf{q}'). \quad (26)$$

To test the two-electron continuum functions  $\phi_q^{sl}$  obtained in this way, we form overlaps with the target states, of the same symmetry, obtained by the diagonalization (5). For arbitrary  $\epsilon_q$  only the true frozen-core discrete eigenstates will be orthogonal to the calculated continuum functions. By taking  $\epsilon_q = \epsilon_n^N$  we find that we have orthogonality of  $\phi_q^{sl}$  with all states except for the  $\phi_n^N$  state. The overlap with the latter increases with the size of the basis and is in excess of unity in typical calculations whereas the overlaps with the other states are  $< 10^{-3}$ .

When considering  $\langle \phi_q^{sl} | \phi_n^{Nsl} \rangle$  with  $\epsilon_q = \epsilon_n^N$  for a number of  $n$  we find that this overlap diminishes slightly with increasing  $\epsilon_n^N$ . This is due to the fact that the separation be-

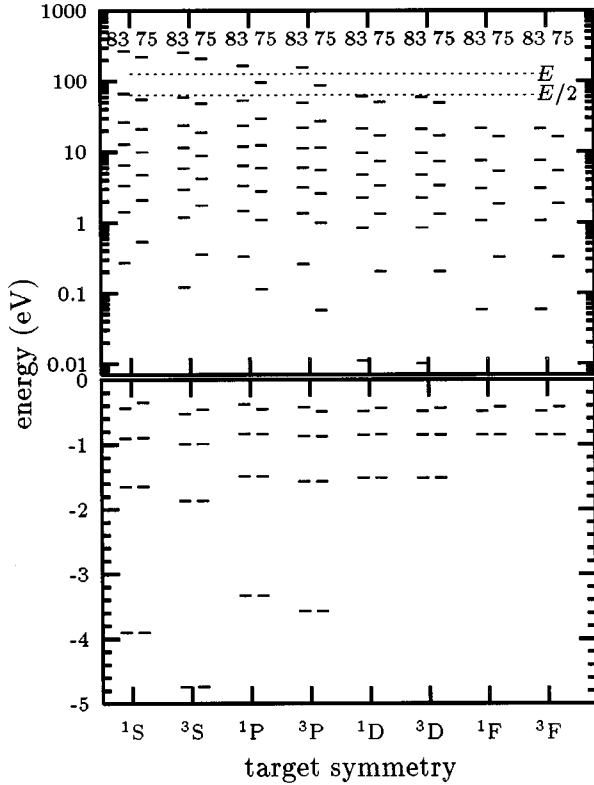


FIG. 1. The excited-state energies (above core) arising in the 75- and 83-state  $e$ -He calculations. The total energy  $E$  is for incident electrons with energy 150 eV.

tween consecutive  $\epsilon_n^N$  increases with increasing  $\epsilon_n^N$  [see Fig. 1], resulting in the highest-energy state representing the largest-energy range of the true target continuum.

Note that the frozen-core one-electron orbitals (either continuum or bound) for the singlet  $S$  symmetry are not orthogonal to each other or to the  $\text{He}^+ 1s$  orbital. However, by construction, all two-electron target states are orthogonal.

The frozen-core approach adopted here is an improvement over the simple Coulomb-wave ( $Z=1$ ) description of the ejected electron. It is also an improvement on the approach adopted by Schlemmer *et al.* [29] and by Franz and Altick [30], who calculated the ejected electron continuum wave in the static field of the  $\text{He}^+$  ion. This corresponds to setting the right-hand side of Eq. (21) to zero, neglecting electron-electron correlations due to exchange. Our method of calculation of the continuum wave functions leads to essentially the same wave functions as those calculated by Furtado and Mahony [31] using the  $R$ -matrix method. Schwienhorst *et al.* [32] went further by relaxing the frozen-core approximation, which allows for the calculation of resonant phenomena.

### C. Generation of ionization cross sections

We use the  $(e, 2e)$  ionization amplitude (14) to calculate the triple-differential cross section (TDCS) for the ionization by electron impact. In atomic units it is given by

$$\frac{d\sigma^S(\mathbf{k}, \mathbf{q})}{d\Omega_k d\Omega_q de} = (2\pi)^4 \frac{kq}{k_i} \sum_s |f_s^{SN}(\mathbf{k}, \mathbf{q})|^2, \quad (27)$$

where  $k_i, k, q$  are the momenta of the incident, scattered (primary) and ejected electrons, respectively, and  $e = q^2/2$  is the ejected-electron energy. The collision frame with the  $z$  axis chosen along the direction of the incident electron and the scattering plane defined by the incident and scattered (primary) electrons is used. The spherical coordinates  $(\theta_p, \phi_p = 0)$  of the primary and  $(\theta_e, \phi_e)$  of the ejected electrons define the scattering geometry.

Double-differential cross sections (DDCS) can be obtained by integration of the TDCS over the spherical coordinates of one of the continuum electrons. In this way different DDCS are formed for the ejected and primary electrons. The former one is calculated by integration of the TDCS over the coordinates of the primary electron and can be calculated by

$$\begin{aligned} \frac{d\sigma_e^S(\mathbf{q})}{d\Omega_q de} &= (2\pi)^4 \frac{kq}{k_i} \sum_s \sum_{l, l' \leq l, m} \frac{2}{1 + \delta_{l'l}} Y_{lm}(\hat{\mathbf{q}}) Y_{l'm}^*(\hat{\mathbf{q}}) \\ &\times \text{Re} \left[ (-i)^{l+l'} \int d\Omega_k f_{slm}^{SN}(\mathbf{k}, \mathbf{q}) f_{s'l'm}^{*SN}(\mathbf{k}, \mathbf{q}) \right]. \end{aligned} \quad (28)$$

The latter one is obtained by integration of the TDCS over the coordinates of the ejected electron (this can be done analytically) and is given by

$$\frac{d\sigma_p^S(\mathbf{k})}{d\Omega_k de} = (2\pi)^4 \frac{kq}{k_i} \sum_s \sum_{l, m} |f_{slm}^{SN}(\mathbf{k}, \mathbf{q})|^2. \quad (29)$$

Note that this DDCS describes the primary electron with energy  $e = k^2/2 = E - q^2/2$ .

The single-differential cross section (SDCS) is obtained by integration of the DDCS for either ejected or primary electrons over the remaining spatial coordinates

$$\frac{d\sigma^S(e)}{de} = (2\pi)^4 \frac{kq}{k_i} \sum_s \sum_{l, m} \int d\Omega_k |f_{slm}^{SN}(\mathbf{k}, \mathbf{q})|^2. \quad (30)$$

This cross section gives the probability of the ejected electron having energy  $e = q^2/2$ , or, equivalently, the primary electron having energy  $e = k^2/2$ .

Finally, the total ionization cross section (TICS) is obtained by integration of the SDCS over the ejected (primary) electron energy:

$$\begin{aligned} \sigma_i^S &= \int_0^E de \frac{d\sigma^S(e)}{de} \\ &= (2\pi)^4 \int_0^E de \frac{kq}{k_i} \sum_s \sum_{l, m} \int d\Omega_k |f_{slm}^{SN}(\mathbf{k}, \mathbf{q})|^2. \end{aligned} \quad (31)$$

Due to the discretization of the target continuum in our approach, the SDCS is known only at a number of points corresponding to the positions of the positive-energy states  $\phi_n^{Nsl}$ . To perform the integration over  $e$  in (31), we therefore have to interpolate the available SDCS. The quality of the interpolation can be checked by comparing with the TICS obtained by summation over the integrated cross sections for the excitation of the positive-energy states [24].

All formulas for cross sections have been written for particular total spin  $S$ . The spin-averaged cross sections are ob-

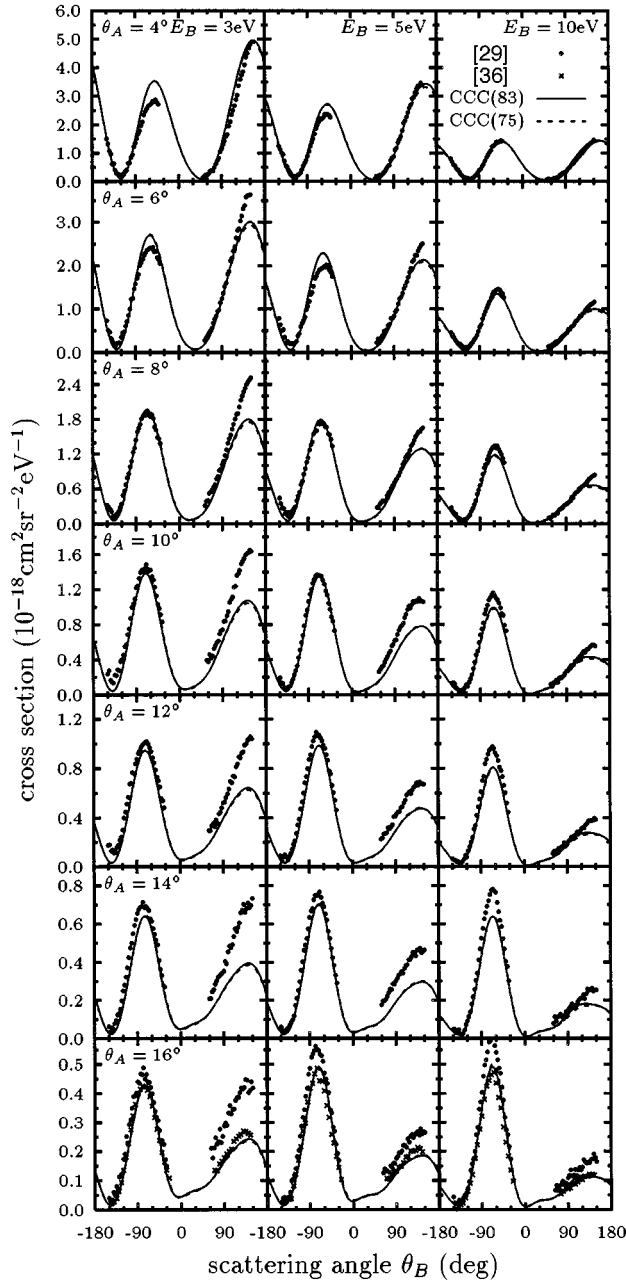


FIG. 2. Electron-impact ionization of helium TDCS at 150 eV. The CCC(83) and CCC(75) calculations are described in the text. The measurements denoted by SSRE91 and Röder96 are due to Schlemmer *et al.* [29] and Röder [36], with the latter being normalized to the CCC calculations at the binary maximum.

tained by summing the cross sections for particular total spin  $S$  multiplied by the corresponding spin weights. For hydrogenic targets,

$$\sigma_i = \sigma_i^0/4 + 3\sigma_i^1/4, \quad (32)$$

and  $s$  in (27)–(31) takes the single value of  $1/2$ . For helium-like target ground-state ionization  $S=1/2$  only, but  $s$  in (27)–(31) takes the values of 0 for singlet and 1 for triplet states.

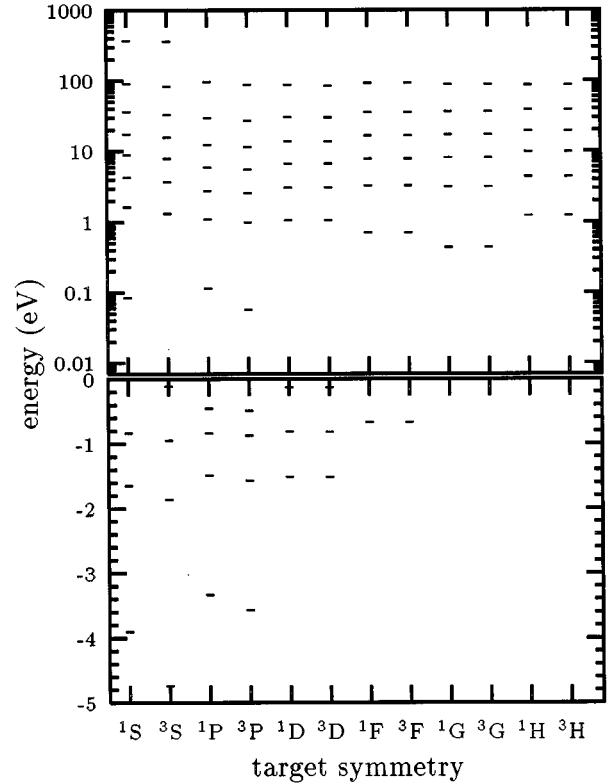


FIG. 3. The excited-state energies (above core) arising in the 101-state  $e$ -He calculations.

The summation over  $l$  in (14) and (28)–(31) is up to the maximum value  $l_{\max}$  of the target-space orbital angular momentum included in the close-coupling expansion (within the projection operator  $I^N$ ). This specifies the maximum orbital angular momentum of the ejected electron. The  $l_{\max}$  value is relatively small ( $l_{\max} \leq 5$ ) when compared to the allowed maximum orbital angular momentum of the primary electron, which can be formally taken to infinity if the analytical Born subtraction is used to calculate the scattering amplitudes  $f_n^{SN}(\mathbf{k})$ . Primary and ejected electrons, therefore, are not treated symmetrically, which is a general feature of any close-coupling formulation. For this reason we find that we have to sum cross sections for theoretically distinguishable but experimentally indistinguishable processes.

Let us begin with the TDCS (27). It specifies the ionization process with total energy  $E = q^2/2 + k^2/2$ , where the primary electron has momentum  $\mathbf{k}$  and the ejected electron has momentum  $\mathbf{q}$ . Another ionization process at the same total energy  $E$ , where the primary electron has momentum  $\mathbf{q}$  and the ejected electron has momentum  $\mathbf{k}$ , cannot be experimentally distinguished from the former one. Therefore, we sum the cross sections for these two processes in order to compare with experiment, i.e.,

$$\frac{d\sigma_i^S(\mathbf{k}, \mathbf{q})}{d\Omega_k d\Omega_q de} = \frac{d\sigma^S(\mathbf{k}, \mathbf{q})}{d\Omega_k d\Omega_q de} + \frac{d\sigma^S(\mathbf{q}, \mathbf{k})}{d\Omega_k d\Omega_q de}. \quad (33)$$

This summation is not related to antisymmetry and needs to be implemented whether or not exchange is included in the close-coupling calculations. For highly asymmetric energy

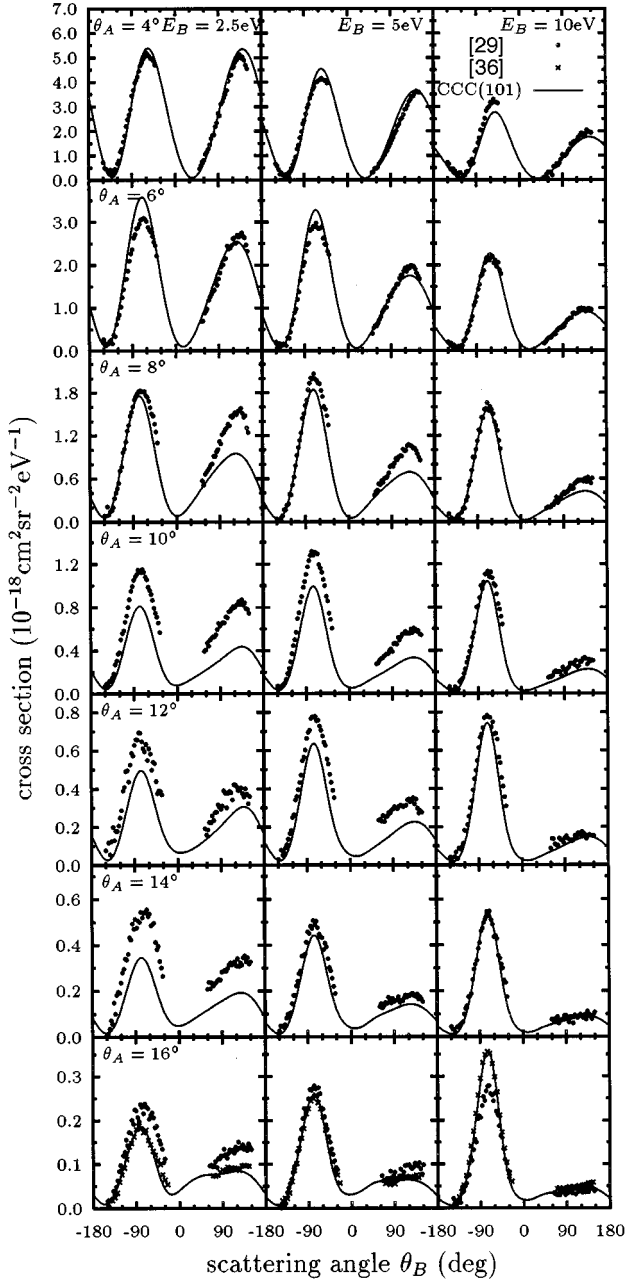


FIG. 4. Electron-impact ionization of helium TDCS at 250 eV. The CCC(101) calculation is described in the text. The measurements denoted by SSRE91 and Röder96 are due to Schlemmer *et al.* [29] and Röder [36], with the latter being normalized to the CCC calculations at the binary maximum.

sharing ( $k \gg q$ ) the first process will be dominant, whereas for equal energy sharing ( $k \approx q$ ) both processes become comparable.

Let us now consider the DDCS. Experimentally, this is obtained by observation of an electron with momentum  $\mathbf{k}$ . Both primary and ejected electrons contribute, therefore resulting in

$$\frac{d\sigma_i^S(\mathbf{k})}{d\Omega_k de} = \frac{d\sigma_e^S(\mathbf{k})}{d\Omega_k de} + \frac{d\sigma_p^S(\mathbf{k})}{d\Omega_k de}. \quad (34)$$

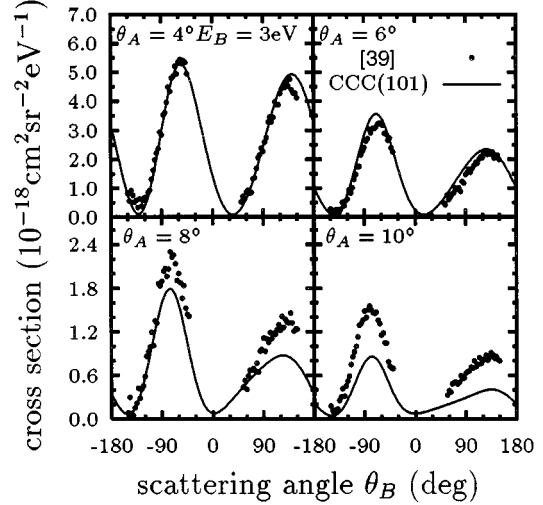


FIG. 5. Electron-impact ionization of helium TDCS at 250 eV. CCC(101) calculations are described in text. The measurements denoted by MSJE85 are due to Müller-Fiedler *et al.* [39].

The same result can be obtained by integration of (33) over the spherical coordinates of either the primary or the ejected electron.

The SDCS is related to the detection probability of an electron with energy  $e$ . Again, both primary and ejected electrons will contribute and the experimentally registered SDCS is given by

$$\frac{d\sigma_i^S(e)}{de} = \frac{d\sigma^S(e)}{de} + \frac{d\sigma^S(E-e)}{de}. \quad (35)$$

The TICS is now given by

$$\begin{aligned} \sigma_i^S &= \int_0^E de \frac{d\sigma^S(e)}{de} \\ &= \int_0^{E/2} de \frac{d\sigma_i^S(e)}{de}. \end{aligned} \quad (36)$$

This is the experimental definition with the upper integration limit  $E/2$  used to avoid double counting.

### III. RESULTS

The primary aim of this paper is to present the detailed formalism of the CCC method for the calculation of electron-impact ionization. In the preliminary  $e$ -He at 100 eV work [18] we showed that the CCC method accurately obtained elastic and excitation differential cross sections of the helium ground state to the  $n \leq 3$  states, as well as the total, single-, double-, and triple-differential cross sections. We now apply the above techniques to the calculation of the  $e$ -He ionization cross sections at higher energies, primarily for completeness. At these energies many other approaches to ionization work very well, and it is not practical for us to compare with them all. Instead, we shall concentrate on providing a comprehensive set of CCC results for the cases where measurements exist in the asymmetric kinematics region. The symmetric kinematical region is numerically too difficult since, at high

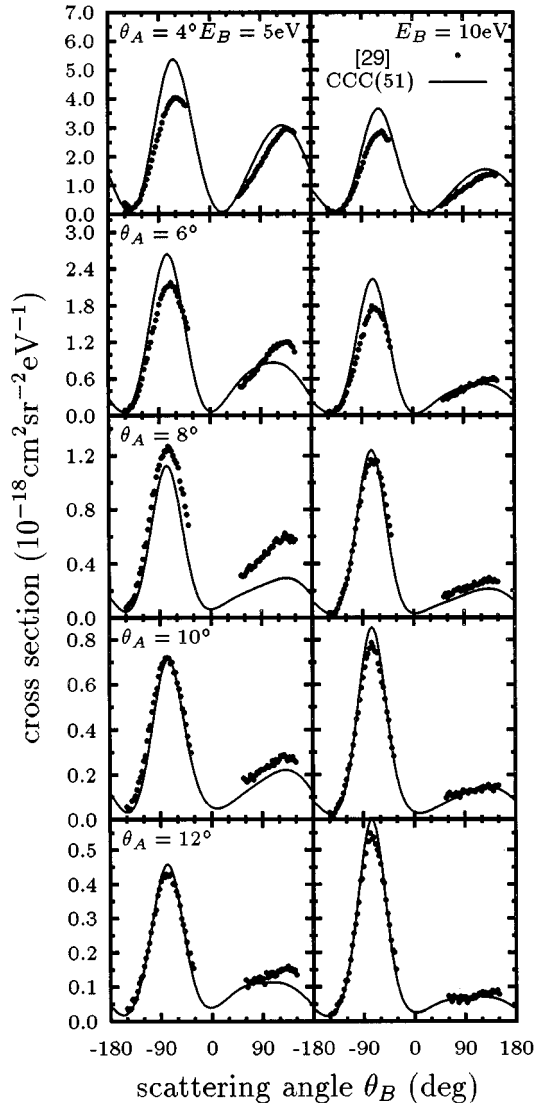


FIG. 6. Electron-impact ionization of helium TDCS at 400 eV. CCC(51) calculations are described in text. The measurements denoted by SSRE91 are due to Schlemmer *et al.* [29].

incident energies, this requires accurate determination of excitation of very high-energy states  $\phi_n^N$ . Furthermore, at the high incident energies, equal-energy-sharing cross sections are particularly small. The size of our calculations would become prohibitively large if enough states were taken, in the required target symmetries, to accurately cover this energy region (see discussion below). The distorted-wave approaches of Whelan, Allan, and Walters [33] and Zhang, Whelan, and Walters [34] appear to do very well here.

Generally, a single CCC calculation yields most accurately the largest cross sections of the scattering system. The bigger the calculation the more of the smaller cross sections will be accurately obtained.

#### A. Triple differential cross sections

In Fig. 1 we give the energy levels of the 75- and 83-state calculations for  $e$ -He ionization at 150 eV. Both include target states with  $l \leq 3$ , with the difference being that for each

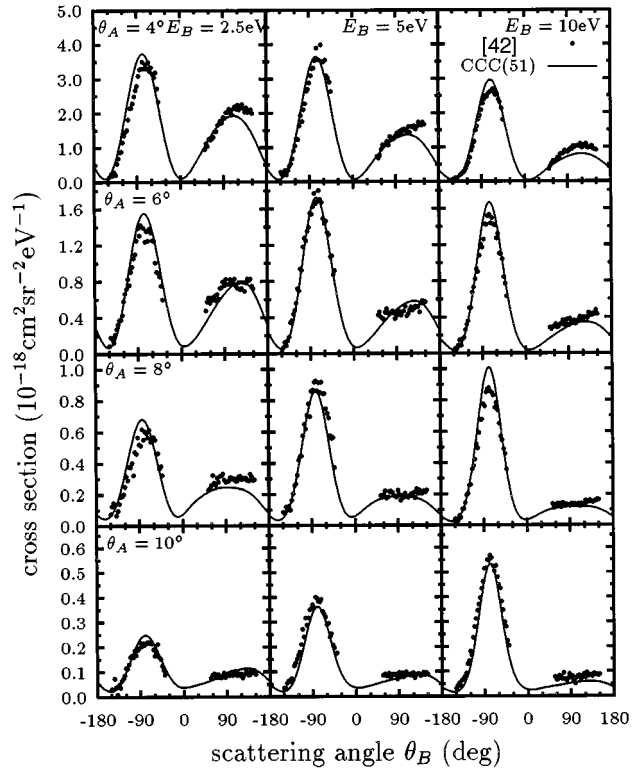


FIG. 7. Electron-impact ionization of helium TDCS at 600 eV. CCC(51) calculations are described in text. The measurements denoted by JMSEK85 are due to Jung *et al.* [42].

given target symmetry there is one more state in the larger calculation. This figure shows how the energy levels move with increasing basis size. The discrete spectrum only varies for the higher excited states, whereas the continuum has a completely different rearrangement with the larger set spanning the continuum more extensively. Also given are the total energy  $E$  (above core) and  $E/2$  to indicate that most of the states have energies below  $E/2$ , indicating the difficulty of obtaining accurate TDCS results in the equal-energy-sharing region at this and higher incident energies.

The results of the 75- and 83-state calculations for  $e$ -He ionization at 150 eV are given in Fig 2. The coplanar measurements by Schlemmer *et al.* [29] have been normalized to the second Born approximation of Srivastava and Sharma [35]. The fast electron with energy  $E_A$  is detected at the given angles  $\theta_A$  in coincidence with the slow electron of given energy  $E_B$  being detected at  $\theta_B$ . Generally, agreement with experiment is good, though on occasion there are substantial discrepancies with our calculations, which show good convergence. For this reason we requested that new measurements be performed, which at the time was only possible at the largest scattering angle  $\theta_A = 16^\circ$ . The relative measurements of Röder [36] have been normalized to the CCC calculations at the binary maximum and show much better agreement in shape with our calculations than the earlier measurements. We are confident of the accuracy of our results at smaller values of  $\theta_A$ . Jones *et al.* [37] and Biswas and Sinha [38] have presented comparison of their three-body theories with some of the data [29] showing good agreement. In these cases, so do our calculations.

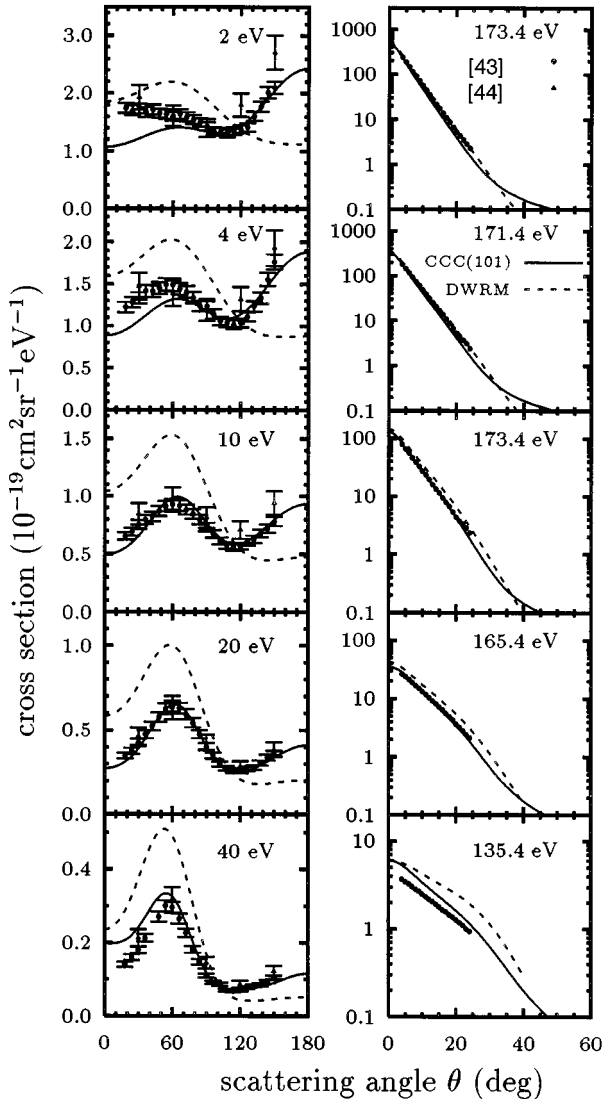


FIG. 8. Electron-impact ionization of helium DDCS at 200 eV. CCC(101) calculations are described in text. The calculations denoted by DWRM are due to Schwienhorst *et al.* [32]. The measurements denoted by MJE86 and GB86 are due to Müller-Fiedler, Jung, and Ehrhardt [43] and Goruganthu and Bonham [44], respectively.

In Fig. 3 we present the energy levels arising in the 101-state calculation used at a number of high energies. We found that convergence is relatively easy to achieve at the considered ejected-electron energies, and so we use just a single (our largest) calculation for presentation. This calculation includes target states with angular momentum  $l \leq 5$ .

The results of the 101-state calculation for incident energy of 250 eV are given in Fig. 4. The measurements of Schlemmer *et al.* [29] were put on an absolute scale by extrapolating the generalized oscillator strength to the optical-dipole oscillator strength known from photoionization experiments. Agreement between the CCC theory and experiment is similar in quality to that at 150 eV. Some very good quantitative agreement can be seen on occasion, and some very poor also. The measurements of Röder [36] for  $\theta_A = 16^\circ$  are once more in excellent agreement with our calculations, giving us con-

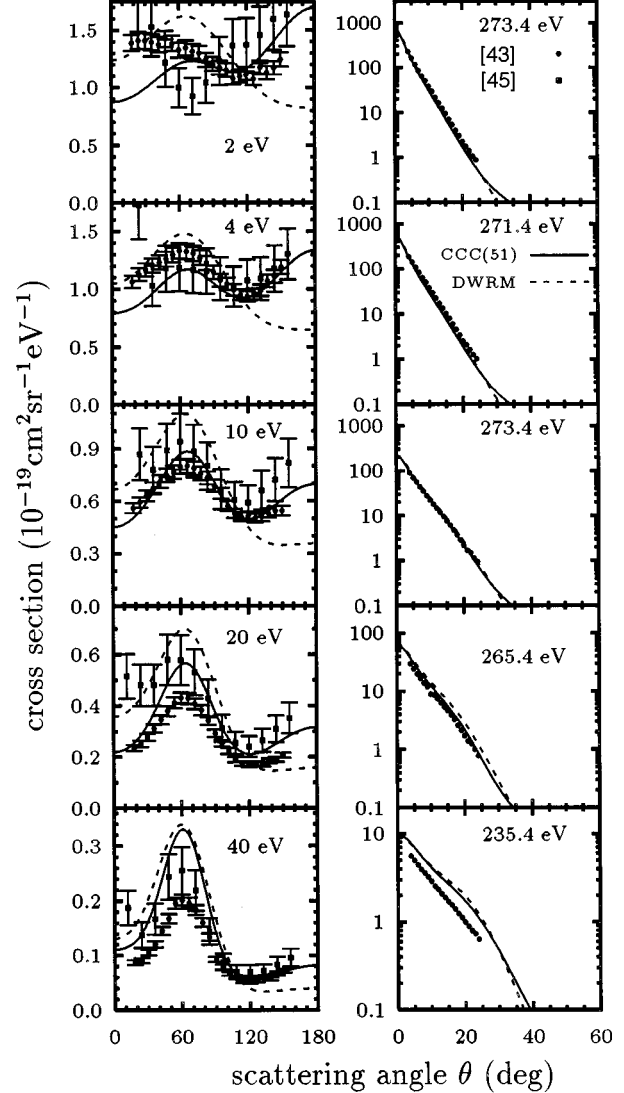


FIG. 9. Electron-impact ionization of helium DDCS at 300 eV. CCC(51) calculations are described in text. The calculations denoted by DWRM are due to Schwienhorst *et al.* [32]. The measurements denoted by MJE86 and SS79 are due to Müller-Fiedler, Jung, and Ehrhardt [43] and Shyn and Sharp [45], respectively.

fidence in the accuracy of our results for other  $\theta_A$ . The results of the above-mentioned three-body theories are also available for selected cases where agreement with our calculations is satisfactory.

We find a similar situation at 256 eV, presented in Fig. 5. The measurements of Müller-Fiedler *et al.* [39] have also been normalized using oscillator strengths. Our 101-state results are in fact quite similar to the second-order calculations of Byron, Joachain, and Piraux [40] and of Furtado and O'Mahony [41]. So again we are confident of our results.

At 400 eV we find that we may drop exchange from our calculation and so omit the triplet states. This reduces the 101-state calculation by 50 states. The singlet energy levels are the same as in Fig. 3. The 51-state results are given in Fig. 6. The data are due to Schlemmer *et al.* [29]. Here we find generally somewhat better agreement with experiment, though on occasion there are substantial discrepancies that we are unable to explain.

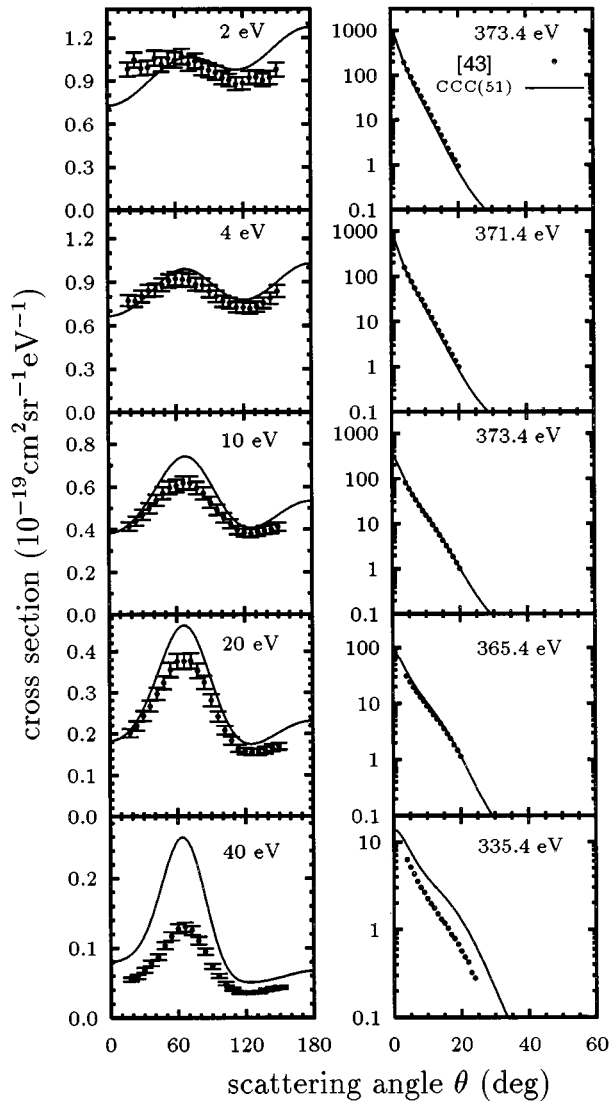


FIG. 10. Electron-impact ionization of helium DDCS at 400 eV. CCC(51) calculations are described in text. The measurements denoted by MJE86 are due to Müller-Fiedler, Jung, and Ehrhardt [43].

The same 51-state calculation is applied at 600 eV and the results are in excellent agreement with all the measurements by Jung *et al.* [42], presented in Fig. 7. We find this encouraging and believe that our 400-eV data are equally reliable.

### B. Double-differential cross sections

We now turn to the presentation of the double-differential cross sections from our CCC calculations. Our DDCS at 200 eV are presented in Fig. 8. The 101-state results are in reasonably good agreement with the measurements of Müller-Fiedler, Jung, and Ehrhardt [43] and those of Goruganthu and Bonham [44]. Note that the figure is arranged in DDCS pairs of the slow and the corresponding fast electron. The integral over these cross sections must be the same. For this reason we suspect that the bottom pair of experimental DDCS are not consistent with each other. We are also puzzled as to why the agreement at small scattering angles improves with higher energy of the slow detected electron.

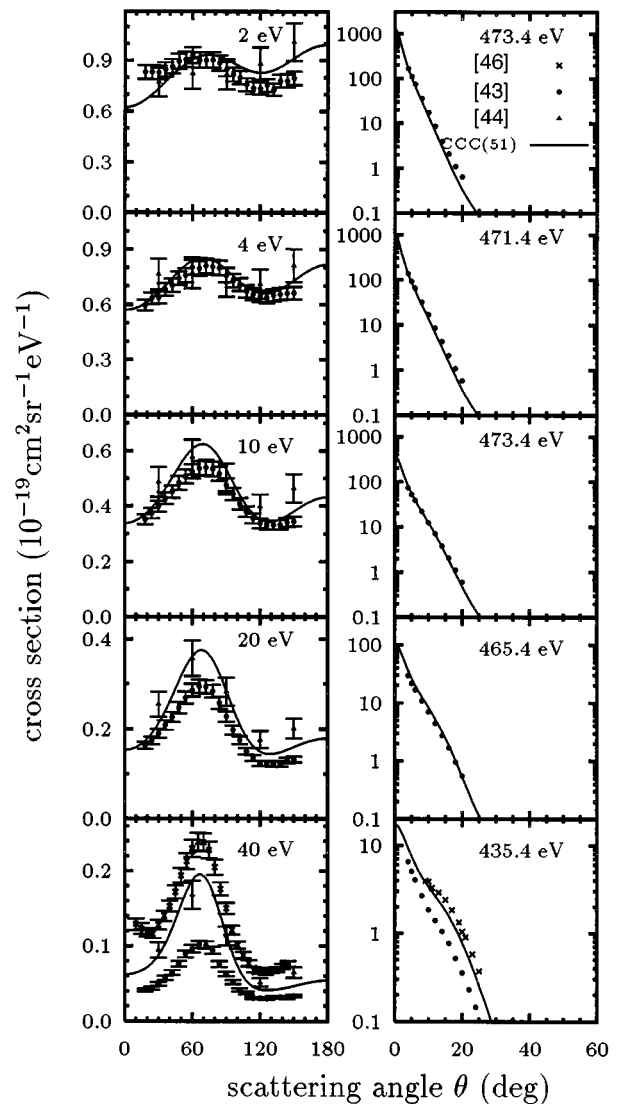


FIG. 11. Electron-impact ionization of helium DDCS at 500 eV. CCC(51) calculations are described in text. The measurements denoted by MJE86, GB86, and ACFS87 are due to Müller-Fiedler, Jung, and Ehrhardt [43], Goruganthu and Bonham [44], and Avaldi *et al.* [46], respectively.

Our results are an improvement over the distorted-wave calculations of Schwienhorst *et al.* [32], particularly for the slow-electron DDCS. They used *R*-matrix techniques for generating the target continuum waves, and so have a similar description of the target structure. The difference in the calculations indicates that the CCC method treats the scattering more accurately.

The 300-eV DDCS are presented in Fig. 9. In addition to the measurements of Müller-Fiedler, Jung, and Ehrhardt [43] we present the measurements by Shyn and Sharp [45]. At this energy we have dropped exchange in our calculation and so only the 51 singlet states (see Fig. 3) were included. The CCC calculation is usually in agreement with at least one set of measurements. However, the problem at small scattering angles for the 2-eV detected electron persists. Apart from the presented distorted-wave calculation [32], the three-body-

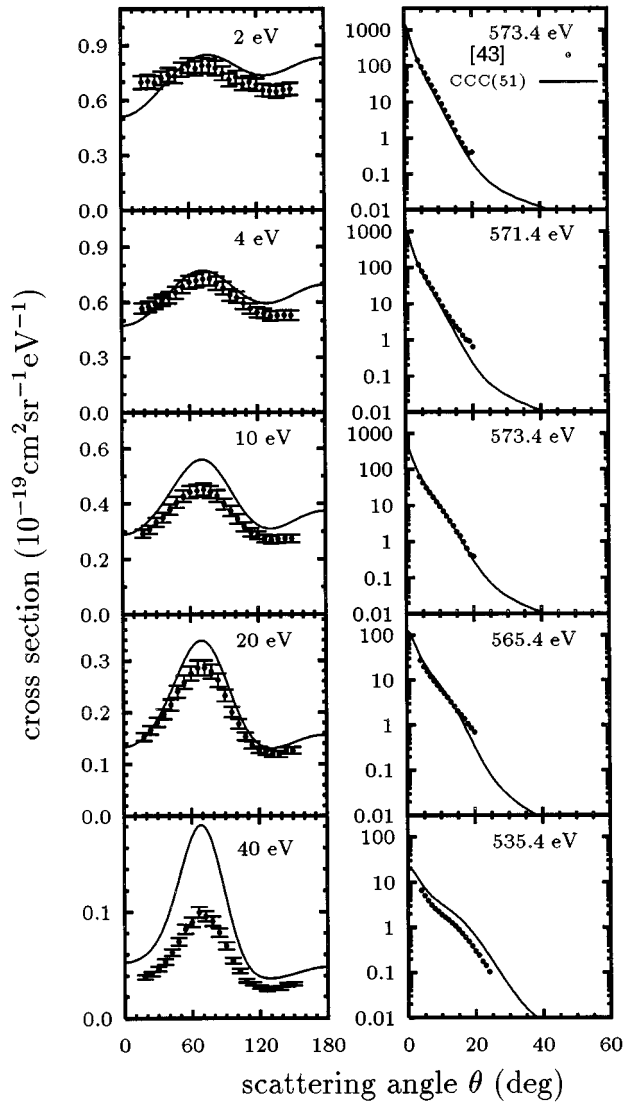


FIG. 12. Electron-impact ionization of helium DDCS at 600 eV. CCC(51) calculations are described in text. The measurements denoted by MJE86 are due to Müller-Fiedler, Jung, and Ehrhardt [43].

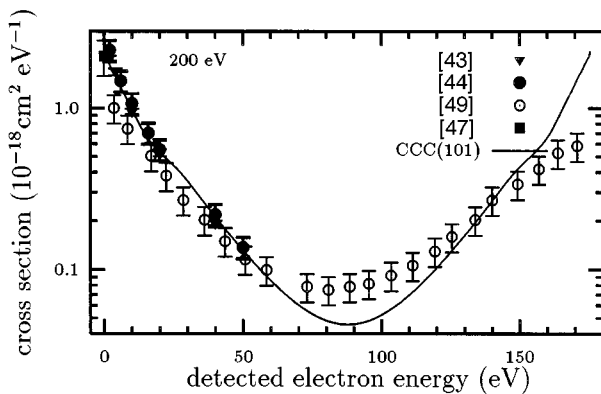


FIG. 13. Electron-impact ionization of helium SDCS at 200 eV. CCC(101) calculations are described in text. The measurements denoted by MJE86, GB86, RD77, and GCG72 are due to Müller-Fiedler, Jung, and Ehrhardt [43], Goruganthu and Bonham [44], Rudd and DuBois [49], and Grissom *et al.* [47], respectively.

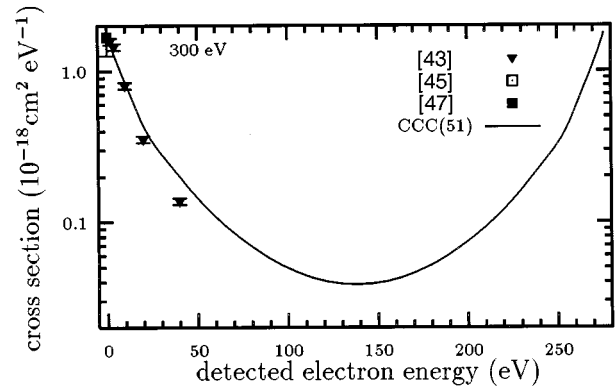


FIG. 14. Electron-impact ionization of helium SDCS at 300 eV. CCC(51) calculations are described in text. The measurements denoted by MJE86, SS79, and GCG72 are due to Müller-Fiedler *et al.* [43], Shyn and Sharp [45], and Grissom, Compton, and Garrett [47], respectively.

theory results of Biswas and Sinha [38] are available and somewhat similar to our results.

In Fig. 10 we present DDCS results at 400 eV. We are only aware of the measurements of Müller-Fiedler, Jung, and Ehrhardt [43] at this energy. The same 51 states were used in the CCC calculation as for 300 eV. Agreement with the measurements is quite good, perhaps with the exception of the 2-eV case. For the bottom pair of energies, though the shape is in good agreement with experiment [43], the absolute value is not. This systematic trend is also evident in the following figure (Fig. 11) for the 500-eV case, where there are measurements due to Goruganthu and Bonham [44] and Avaldi *et al.* [46]. The latter two sets are in better agreement with our calculation and gives us confidence in the accuracy of all of our presented DDCS for the detected electron with 40-eV energy.

The 600-eV DDCS are presented in Fig. 12. Here the agreement of the 51-state calculation with the data of Müller-Fiedler, Jung, and Ehrhardt [43] is of similar quality as that for the lower energies.

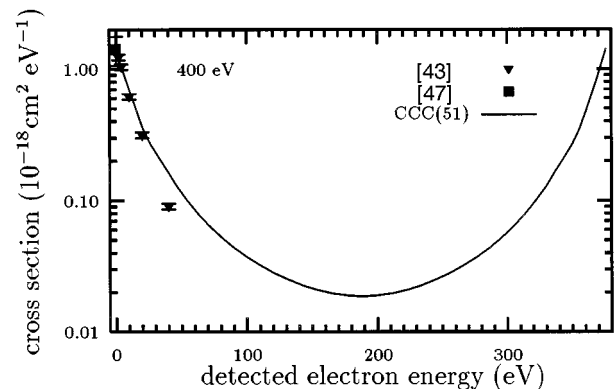


FIG. 15. Electron-impact ionization of helium SDCS at 400 eV. CCC(51) calculations are described in text. The measurements denoted by MJE86 and GCG72 are due to Müller-Fiedler, Jung, and Ehrhardt [43] and Grissom *et al.* [47], respectively.

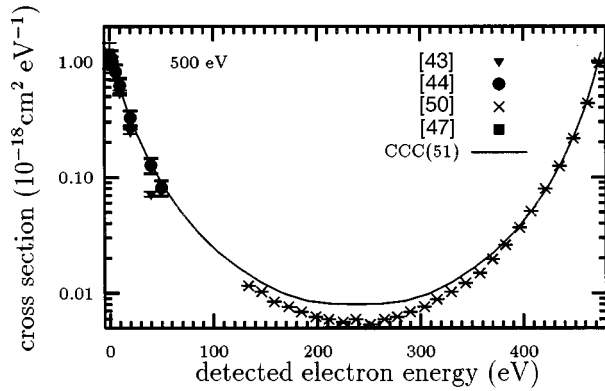


FIG. 16. Electron-impact ionization of helium SDCS at 500 eV. CCC(51) calculations are described in text. The measurements denoted by MJE86, GB86, Oda75, and GCG72 are due to Müller-Fiedler, Jung, and Ehrhardt [43], Goruganthu and Bonham [44], Oda [50], and Grissom *et al.* [47], respectively.

### C. Single-differential cross sections

We now turn to the presentation of the single-differential cross sections. These are obtained by angular integration of the DDCS. This is the case in both theory and experiment except for the single zero-energy measurement of Grissom, Compton, and Garrett [47]. As such, generally the SDCS do not provide any more information than has been discussed above. We present them primarily for completeness and to show the results of those measurements whose DDCS we did not give above for clarity of presentation.

The SDCS results are presented in Figs. 13–17. Agreement with most of the available measurements is very good. Sometimes this is even the case when there is some discrepancy between the theoretical and experimental DDCS, with the integration hiding this information. On occasion some of the systematic discrepancies with the DDCS measurements may be seen even after integration has been performed.

## IV. CONCLUSIONS

We have presented detailed theory for the calculation of differential ionization within the close-coupling formalism, and together with our earlier work [18], have applied it systematically at energies 100 eV and above to  $e$ -He ionization. This application has enabled a detailed examination of the available experimental data. We believe that on occasion our results are more accurate than experiment. We claim this because the CCC formalism for  $(e,2e)$  should be quite accurate in the asymmetric kinematic region at intermediate to high incident energies. Whereas one may argue about the validity of taking a charged continuum wave and a plane wave for the outgoing electrons in the case of equal excess-energy sharing, this is certainly justifiable in the highly asymmetric kinematic region. We also note that in the calculations performed here the frozen-core approximation has been used for both the target discrete and continuous spectra. As in the case of discrete excitation [10], we believe that this is not a significant approximation for the considered cases.

The primary strength of the CCC theory over other tech-

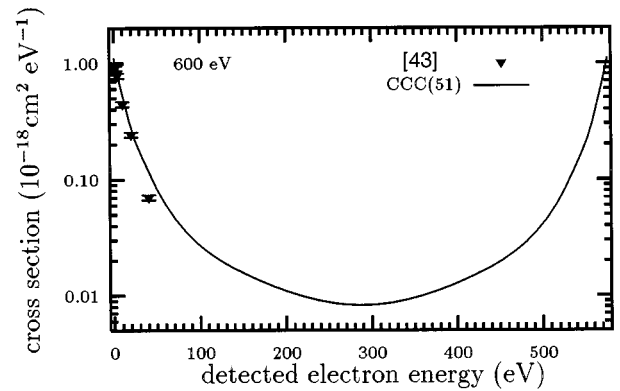


FIG. 17. Electron-impact ionization of helium SDCS at 600 eV. CCC(51) calculations are described in text. The measurements denoted by MJE86 are due to Müller-Fiedler, Jung, and Ehrhardt [43].

niques is that the total wave function of the scattering system is able to be determined *ab initio* utilizing relatively large-basis expansions. The formalism ensures that the results are the same whether the projectile is treated as a plane or a distorted wave, which is often not the case in the distorted-wave approximations. Even with the historically large number of states it is important to keep in mind that for each target symmetry the infinite sum over true discrete states and an integral over the true target continuum is represented by only a handful (ten or so) of square-integrable states. For this reason accurate determination of relatively small cross sections (e.g.,  $n \geq 4$  excitation, equal-energy-sharing ionization cross sections with high incident energies) require even larger calculations.

In this work the CCC method has been applied to the high incident energies. From the theoretical standpoint we are particularly interested in applying the formalism at intermediate to low energies, where we expect to encounter more difficulties. Initial applications [14,15] at 50 and 40 eV show encouraging agreement for the asymmetric kinematics, but show some problems in the equal- or near-equal-energy-sharing region. It is on this area that we shall concentrate in the future. We are also confident that the same formalism may be applied to the calculation of  $(\gamma,2e)$  processes. This has been demonstrated already for the calculation of total double photoionization of helium [48]. In time we shall look at differential cross sections for the latter process.

## ACKNOWLEDGMENTS

We thank Jochen Röder for his considerable time and effort in performing measurements upon request, and the many detailed and very helpful communications. We are also indebted to Klaus Bartschat for a detailed critique of the manuscript and many helpful suggestions. The support of the Australian Research Council and The Flinders University of South Australia is gratefully appreciated. Research was sponsored in part by the Phillips Laboratory, Air Force Material Command, USAF, under cooperative agreement number F29601-93-2-0001.

- [1] B. Bederson, *Comments At. Mol. Phys.* **1**, 41 (1969).  
[2] B. Bederson, *Comments At. Mol. Phys.* **1**, 65 (1969).  
[3] I. Bray and A. T. Stelbovics, *Phys. Rev. A* **46**, 6995 (1992).  
[4] J. Callaway, *Phys. Rev. A* **32**, 775 (1985).  
[5] W. L. van Wyngaarden and H. R. J. Walters, *J. Phys. B* **19**, 929 (1986).  
[6] D. A. Konovalov and I. E. McCarthy, *J. Phys. B* **27**, L407 (1994).  
[7] K. Bartschat *et al.*, *J. Phys. B* **29**, 115 (1996).  
[8] I. Bray and A. T. Stelbovics, *Phys. Rev. Lett.* **69**, 53 (1992).  
[9] I. Bray, *Phys. Rev. A* **49**, 1066 (1994).  
[10] D. V. Fursa and I. Bray, *Phys. Rev. A* **52**, 1279 (1995).  
[11] I. Bray, *Phys. Rev. Lett.* **73**, 1088 (1994).  
[12] I. Bray and A. T. Stelbovics, *Phys. Rev. Lett.* **70**, 746 (1993).  
[13] I. Bray, D. A. Konovalov, I. E. McCarthy, and A. T. Stelbovics, *Phys. Rev. A* **50**, R2818 (1994).  
[14] J. Röder *et al.*, *J. Phys. B* **29**, L67 (1996).  
[15] J. Röder *et al.*, *J. Phys. B* **29**, 2103 (1996).  
[16] E. P. Curran and H. R. J. Walters, *J. Phys. B* **20**, 337 (1987).  
[17] E. P. Curran, C. T. Whelan, and H. R. J. Walters, *J. Phys. B* **24**, L19 (1991).  
[18] I. Bray and D. V. Fursa, *Phys. Rev. Lett.* **76**, 2674 (1996).  
[19] I. Bray and A. T. Stelbovics, *Adv. Atom. Mol. Phys.* **35**, 209 (1995).  
[20] A. T. Stelbovics, *Phys. Rev. A* **41**, 2536 (1990).  
[21] I. Bray and A. T. Stelbovics, *Comp. Phys. Commun.* **85**, 1 (1995).  
[22] M. R. H. Rudge, *Rev. Mod. Phys.* **40**, 564 (1968).  
[23] M. Brauner, J. S. Briggs, and H. Klar, *J. Phys. B* **22**, 2265 (1989).  
[24] I. Bray and D. V. Fursa, *J. Phys. B* **28**, L435 (1995).  
[25] I. E. McCarthy and A. T. Stelbovics, *Phys. Rev. A* **28**, 2693 (1983).  
[26] L. V. Chernysheva, N. A. Cherepkov, and V. Radojevic, *Comp. Phys. Commun.* **11**, 57 (1976).  
[27] M. Cohen and P. S. Kelly, *Can. J. Phys.* **45**, 2079 (1967).  
[28] C. F. Fisher, *The Hartree-Fock Method for Atoms* (Wiley, New York, 1977).  
[29] P. Schlemmer, M. K. Srivastava, T. Rösel, and H. Ehrhardt, *J. Phys. B* **24**, 2719 (1991).  
[30] A. Franz and P. L. Altick, *J. Phys. B* **25**, 1577 (1992).  
[31] F. M. Furtado and P. F. O'Mahony, *J. Phys. B* **20**, L405 (1987).  
[32] R. Schwienhorst, A. Raeker, R.H.G. Reid, and K. Bartschat, *J. Phys. B* **28**, 4651 (1995).  
[33] C. T. Whelan, R. J. Allan, and H. R. J. Walters, *J. Phys.* **3**, 39 (1993).  
[34] X. Zhang, C. T. Whelan, and H. R. J. Walters, *J. Phys. B* **23**, L509 (1990).  
[35] M. K. Srivastava and S. Sharma, *Phys. Rev. A* **37**, 628 (1988).  
[36] J. Röder (private communication).  
[37] S. Jones, D. H. Madison, A. Franz, and P. L. Altick, *Phys. Rev. A* **48**, R22 (1993).  
[38] R. Biswas and C. Sinha, *Phys. Rev. A* **51**, 3766 (1995).  
[39] R. Müller-Fiedler, P. Schlemmer, K. Jung, and H. Ehrhardt, *Z. Phys. A* **320**, 89 (1985).  
[40] F. W. Byron Jr., C. J. Joachain, and B. Piraux, *J. Phys. B* **19**, 1201 (1986).  
[41] F. M. Furtado and P. F. O'Mahony, *J. Phys. B* **21**, 137 (1988).  
[42] K. Jung *et al.*, *J. Phys. B* **18**, 2955 (1985).  
[43] R. Müller-Fiedler, K. Jung, and H. Ehrhardt, *J. Phys. B* **19**, 1211 (1986).  
[44] R. R. Gorughanthu and R. A. Bonham, *Phys. Rev. A* **34**, 103 (1986).  
[45] T. W. Shyn and W. E. Sharp, *Phys. Rev. A* **19**, 557 (1979).  
[46] L. Avaldi, R. Camilloni, E. Fainelli, and G. Stefani, *Nuovo Cimento D* **9**, 97 (1987).  
[47] J. T. Grissom, R. N. Compton, and W. R. Garrett, *Phys. Rev. A* **6**, 977 (1972).  
[48] A. Kheifets and I. Bray, *Phys. Rev. A* (to be published).  
[49] M. E. Rudd and R. D. DuBois, *Phys. Rev. A* **16**, 26 (1977).  
[50] N. Oda, *Radiat. Res.* **64**, 80 (1975).